Atmos. Chem. Phys., 14, 7273–7290, 2014
www.atmos-chem-phys.net/14/7273/2014/
doi:10.5194/acp-14-7273-2014

Atmospheric Chemistry and Physics
Open Access

Simulating the integrated summertime $\Delta^{14}CO_2$ signature from anthropogenic emissions over Western Europe

D. Bozhinova[1], M. K. van der Molen[1], I. R. van der Velde[1], M. C. Krol[1,2], S. van der Laan[3], H. A. J. Meijer[3], and W. Peters[1]

[1]Meteorology and Air Quality Group, Wageningen University, the Netherlands
[2]Institute for Marine and Atmospheric Research Utrecht, Utrecht, the Netherlands
[3]Centre for Isotope Research, University of Groningen, Groningen, the Netherlands

Correspondence to: D. Bozhinova (denica.bozhinova@wur.nl)

Received: 7 November 2013 – Published in Atmos. Chem. Phys. Discuss.: 21 November 2013
Revised: 30 April 2014 – Accepted: 27 May 2014 – Published: 17 July 2014

Abstract. Radiocarbon dioxide ($^{14}CO_2$, reported in $\Delta^{14}CO_2$) can be used to determine the fossil fuel CO_2 addition to the atmosphere, since fossil fuel CO_2 no longer contains any ^{14}C. After the release of CO_2 at the source, atmospheric transport causes dilution of strong local signals into the background and detectable gradients of $\Delta^{14}CO_2$ only remain in areas with high fossil fuel emissions. This fossil fuel signal can moreover be partially masked by the enriching effect that anthropogenic emissions of $^{14}CO_2$ from the nuclear industry have on the atmospheric $\Delta^{14}CO_2$ signature. In this paper, we investigate the regional gradients in $^{14}CO_2$ over the European continent and quantify the effect of the emissions from nuclear industry. We simulate the emissions and transport of fossil fuel CO_2 and nuclear $^{14}CO_2$ for Western Europe using the Weather Research and Forecast model (WRF-Chem) for a period covering 6 summer months in 2008. We evaluate the expected CO_2 gradients and the resulting $\Delta^{14}CO_2$ in simulated integrated air samples over this period, as well as in simulated plant samples.

We find that the average gradients of fossil fuel CO_2 in the lower 1200 m of the atmosphere are close to 15 ppm at a 12 km × 12 km horizontal resolution. The nuclear influence on $\Delta^{14}CO_2$ signatures varies considerably over the domain and for large areas in France and the UK it can range from 20 to more than 500 % of the influence of fossil fuel emissions. Our simulations suggest that the resulting gradients in $\Delta^{14}CO_2$ are well captured in plant samples, but due to their time-varying uptake of CO_2, their signature can be different with over 3 ‰ from the atmospheric samples in some regions. We conclude that the framework presented will be well-suited for the interpretation of actual air and plant $^{14}CO_2$ samples.

1 Introduction

The magnitude of anthropogenic fossil fuel CO_2 emissions is relatively well known on the global scale (Raupach et al., 2007; Friedlingstein et al., 2010) as bottom-up inventories constrain the sum of all emissions to within 6–10 % uncertainty (Marland and Rotty, 1984; Turnbull et al., 2006; Marland, 2008). But it is widely acknowledged that confidence in the estimated magnitude of these emissions reduces quickly when we consider the regional and national scale (Olivier and Peters, 2002; Gurney et al., 2009; Francey et al., 2013). At length scales of 150 km and smaller, bottom-up emission maps can differ up to 50 % (Ciais et al., 2010). This is partly a disaggregation problem that arises when nationally reported data on economic activity, energy use, and fuel trade statistics must be attributed to smaller geographic areas and more diverse processes. At the same time, there is a challenge to aggregate available bottom-up information on the level of individual roads, or power plants, or industrial complexes to a larger scale consistently. In between these two lies an important opportunity for atmospheric monitoring, as it can independently verify the reported emission magnitudes at the intermediate scales, uniquely constrained by the integrating capacity of atmospheric transport.

Several atmospheric monitoring strategies for fossil fuel emissions have been applied in recent years. Most of these use spatiotemporal variations in CO_2 mole fractions (Koffi et al., 2013), often augmented with various other energy related gases such as CO (Levin and Karstens, 2007), NO_x (Lopez et al., 2013), or SF_6 (Turnbull et al., 2006). An advantage of these other gases is that they can be measured continuously and relatively cheaply with commercially available analyzers, of which many have already been deployed. However, one of the disadvantages lies in attribution, as each process induces its own typical ratio of these gases to the atmosphere. An example is the much higher CO / CO_2 ratio produced by traffic emissions than by power plants. Another disadvantage is that not all of these trace gases are direct proxies for fossil fuel CO_2 release as some have totally independent, but co-located sources with the sources of anthropogenic CO_2 emissions. This is in large contrast with the one tracer that is generally considered the "gold standard" for fossil fuel related CO_2 detection: radiocarbon dioxide or $^{14}CO_2$ (Kuc et al., 2003; Levin et al., 2003, 2008; Levin and Karstens, 2007; Levin and Rödenbeck, 2008; Turnbull et al., 2006; Djuricin et al., 2010; Miller et al., 2012), reported usually as $\Delta^{14}CO_2$ (Stuiver and Polach, 1977; Mook and van der Plicht, 1999).

Radiocarbon derives its strength for fossil fuel monitoring from the absence of any ^{14}C in carbon that is much older than the typical half-life time of the radiocarbon -5700 ± 30 years (Roberts and Southon, 2007). This typically applies only to carbon in fossil reservoirs, as other carbon reservoirs are continuously supplied with fresh ^{14}C from exchange with the atmosphere where $^{14}CO_2$ is produced in the stratosphere and upper troposphere (Libby, 1946; Anderson et al., 1947). In the natural carbon balance this ^{14}C would cycle through the atmospheric, biospheric, and oceanic reservoir until it decays. But very large anthropogenic disturbances on this natural cycle come specifically from (a) large scale burning of very old and ^{14}C depleted carbon from fossil reservoirs, the "Suess effect" (Suess, 1955; Levin et al., 1980), and (b) production of highly enriched ^{14}C in CO_2 such as from nuclear bomb tests (Nydal, 1968), or some methods of nuclear power production (McCartney et al., 1988a, b). Samples of $^{14}CO_2$ taken from the atmosphere, but also from the oceans and biosphere that exchange with it, consistently show their dominant influence on the $^{14}CO_2$ budget of the past decades (e.g.: Levin et al., 1989, 2010; Meijer et al., 1996; Nydal and Gislefoss, 1996; Levin and Hesshaimer, 2000; Randerson et al., 2002; Naegler and Levin, 2006; Graven et al., 2012a, b).

Monitoring of atmospheric $^{14}CO_2$ is done through several methods. One commonly applied approach is by absorption of gaseous CO_2 into a sodium hydroxide solution from which the carbon content is extracted for $^{14}C / C$ analysis either by radioactive decay counters, or converted into a graphite target for analysis by accelerator mass spectrometry. The air flowing into the solution typically integrates the absorbed CO_2 with sampling time of days, weeks, or even longer periods. While there is a new technique, which uses integrated flask sampling (Turnbull et al., 2012), the other method generally used is to collect an air sample in a flask, which is filled within less than a minute and thus representative of a much smaller atmospheric time-window. Compared to these, at the other end of the time spectrum is the use of plants to sample $^{14}C / C$ ratios in the atmosphere through their photosynthetic fixation of atmospheric CO_2. Depending on the species these integrate over sampling windows of a full growing season (annual crops, fruits – Shibata et al., 2005; Hsueh et al., 2007; Palstra et al., 2008; Riley et al., 2008; Wang et al., 2013) or longer (trees, tree-rings – Suess, 1955; Stuiver and Quay, 1981; Wang et al., 2012).

An effective monitoring strategy for fossil fuel emissions is likely to take advantage of all methods available to collect ^{14}C samples, and combine these with high resolution monitoring of related gases (e.g. CO, SF_6). Levin and Karstens (2007), van der Laan et al. (2010) and Vogel et al. (2010) already demonstrated the viability of a monitoring method in which observed CO / CO_2 ratios are periodically calibrated with $^{14}CO_2$ to estimate fossil fuel emissions at high temporal resolutions. More recently, this strategy was also employed by Lopez et al. (2013), where additionally the CO_2 / NO_x ratios were used to estimate fossil fuel derived CO_2 from continuous CO and NO_x observations in Paris. Turnbull et al. (2011) showed for the city of Sacramento, that using a combination of $\Delta^{14}CO_2$ and CO observations can reveal structural detail in CO_2 from fossil fuel and biospheric sources that cannot be obtained by CO_2 measurements alone. Van der Laan et al. (2010) and recently Vogel et al. (2013) showed that the agreement between modeled fossil fuel CO_2 estimates and observations of ^{14}C-corrected CO can be further improved by including ^{222}Rn as a tracer for the vertical mixing. Finally, Hsueh et al. (2007) and Riley et al. (2008) used $^{14}C / C$ ratios in corn leaves and C3 grasses to reveal fossil fuel emission patterns on city, state, and national scales. Given so many different methods to use ^{14}C in monitoring strategies, its increasing accuracy, reduction in required sample size, and decreasing costs, it is likely that this tracer will play a more important role in the future of the carbon observing network.

The quantitative estimation of fossil fuel emissions from all of the ^{14}C-based monitoring strategies above requires different methods and emphasizes different terms in the $^{14}CO_2$ budget. For example, interpretation of ^{14}C in air samples from aircraft requires detailed dispersion modeling of surface emissions into a highly dynamic atmosphere, while interpretation of monthly integrated air samples from tall towers requires the inclusion of the re-emergence of old ^{14}C signals after longer turn-over in the oceans and biosphere. In a recent publication (Bozhinova et al., 2013), we showed that the interpretation of growing season integrated plant samples additionally requires simulation of location and weather dependent photosynthetic uptake and plant development patterns. A successful ^{14}C monitoring strategy will thus depend

strongly on our ability to capture these diverse processes on diverse scales.

In this work, we present a newly-built framework designed to interpret $^{14}CO_2$ from different types of samples and from different monitoring strategies. The framework includes atmospheric transport of surface emissions of total CO_2 and $^{14}CO_2$ on hourly scales on a model grid of a few kilometers, but integrates signals up to seasonal time scales and even down into the leaves of growing crops (maize and wheat). Both regional transport and plant growth are based on meteorological drivers that are kept consistent with large-scale weather reanalyses. In addition to fossil fuel signals in the atmosphere and in plants, we simulate the spread of nuclear derived ^{14}C release from major reprocessing plants and from operational nuclear power production plants across Europe based on work of Graven and Gruber (2011). We applied our framework to the European domain for the summer of 2008. After explaining the components of the framework (Sect. 2) we will demonstrate its application (Sect. 3.1), assess the fossil and nuclear derived ^{14}C gradients across Europe (Sect. 3.2), and simulate the signal that will be recorded into annual crops growing across the domain (Sect. 3.3). We will evaluate its potential benefits compared to simpler but less realistic fossil fuel estimation methods from integrated samples alone (Sect. 3.4). We will conclude with a discussion (Sect. 4) of the application of this framework to actual measurements and recommendations for future studies.

2 Methods

2.1 The regional atmospheric CO_2 and $\Delta^{14}CO_2$ budget

The regional CO_2 mole fractions and $\Delta^{14}CO_2$ signature of the atmosphere observed at a particular location are described in Eqs. (1) and (2), following the methodology used by Levin et al. (2003), Turnbull et al. (2006), Hsueh et al. (2007), Palstra et al. (2008) and described thoroughly in Turnbull et al. (2009b). Here the Δ_x and CO_{2x} (or $^{14}CO_{2x}$) indicate the $\Delta^{14}CO_2$ signature of CO_2 (or $^{14}CO_2$) mole fractions of particular origin, expressed in the index as follows: obs – observed at location, bg – background, ff – fossil fuels, p – photosynthetic uptake, r – ecosystem respiration, o – ocean, n – nuclear and s – stratospheric.

$$CO_{2obs} = CO_{2bg} + CO_{2ff} + CO_{2p} + CO_{2r} + CO_{2o} + CO_{2s} \quad (1)$$

$$\Delta_{obs}CO_{2obs} = \Delta_{bg}CO_{2bg} + \Delta_{ff}CO_{2ff} + \Delta_{p}CO_{2p} + \Delta_{r}CO_{2r} + \Delta_{o}CO_{2o} + \Delta_{n}{}^{14}CO_{2n} + \Delta_{s}CO_{2s} \quad (2)$$

Several of the terms in both equations can be omitted or transformed in our study, as described next.

We set $\Delta_p = \Delta_{bg}$ similar to the approach in Turnbull et al. (2006) as the calculation of $\Delta^{14}CO_2$ accounts for changes in the signature of the photosynthesized CO_2 flux due to fractionation. The atmosphere-ocean exchange in the northern Atlantic makes the region generally a sink of carbon (Watson et al., 2009), but we assume that its transport to our domain is uniform and captured by the inflow of background air and thus also carries the signature Δ_{bg}. For the ecosystem respiration and ocean exchange the terms Δ_r and Δ_o can be also written as $\Delta_{bg} + \Delta^{dis}_{bio}$ and $\Delta_{bg} + \Delta^{dis}_{ocean}$, where the disequilibrium terms (Δ^{dis}) describe the difference between the signature of the carbon in the particular reservoir and the current atmospheric background. These differences arise from the past enrichment of the atmosphere with $^{14}CO_2$ from the atmospheric nuclear bomb tests since the 1960s. In the following decades this enrichment was incorporated into the different carbon reservoirs (Levin and Kromer, 1997; Levin and Hesshaimer, 2000) and currently these terms are of dominant importance only in particular regions of the globe. For our domain both terms are considered of much smaller influence than the dominant effect of the fossil fuels and are consequently omitted (Levin and Karstens, 2007; Hsueh et al., 2007; Palstra et al., 2008; Turnbull et al., 2009b; Naegler and Levin, 2009a, b; Levin et al., 2010). Because we currently do not correct for this, the omission of the biospheric disequilibrium in the region and period of our study will likely result in a small bias in our results, as our atmosphere will be less enriched during the period of peak biospheric activity. For the northern hemisphere Turnbull et al. (2006) estimates an overestimation of fossil fuel CO_2 by 0.2–0.5 ppm or up to 1.3 ‰ enrichment in $\Delta^{14}CO_2$ due to this lack of disequilibrium influence, while Levin et al. (2008) evaluates this influence on the observational sites in Germany to be within 0.2 ppm or about 0.5 ‰ enrichment. The intrusion of $^{14}CO_2$-enriched stratospheric air can be of importance for observations in the upper troposphere or higher, however in our case this term can be considered as part of the background, as the stratospheric $^{14}CO_2$ is already well mixed by the time it reaches the lower troposphere.

Most studies ignore the effects of anthropogenic nuclear production of $^{14}CO_2$ on the atmospheric $\Delta^{14}CO_2$ since on the global scale this production averages to the smallest contribution, compared to the other terms (Turnbull et al., 2009a) and few try to quantify and correct for it in observations taken nearby nuclear power plants (Levin et al., 2003). However, Graven and Gruber (2011) showed that the regional influence of a dense nuclear power plant network cannot be ignored. They estimated the potential bias in the recalculation of fossil fuel CO_2 due to nuclear power plant production is on average between 0.5 and 1 ppm for Europe, but the horizontal resolution of their transport model ($1.8^\circ \times 1.8^\circ$) limits the analysis for the regions close to the sources. We note that two of the three existing worldwide spent fuel reprocessing plants are located in Western Europe (SFRP, in La Hague, France and

Sellafield, United Kingdom), which generally have higher than average emissions of $^{14}CO_2$ (McCartney et al., 1988a). Particularly the site of La Hague is estimated to be the largest current point-source of $^{14}CO_2$ emissions in the world, in recent years accounting for more than 10 % of the global budget of nuclear produced $^{14}CO_2$ (Graven and Gruber, 2011). The magnitude of this source and its spatial location close to the major fossil fuel emitters in Europe pose a challenge in estimating the uncertainty with which the method of recalculating fossil fuel CO_2 can be applied in the region.

All these considerations allow us to simplify Eqs. (1) and (2) to Eqs. (3) and (4).

$$CO_{2obs} = CO_{2bg} + CO_{2ff} + CO_{2p} + CO_{2r} \quad (3)$$

$$\Delta_{obs}CO_{2obs} = \Delta_{bg}(CO_{2bg} + CO_{2p} + CO_{2r}) + \Delta_{ff}CO_{2ff} + \Delta_{n}^{14}CO_{2n} \quad (4)$$

The instantaneous $\Delta^{14}CO_2$ signature of the atmosphere is calculated using Eq. (4), using the specific signatures for various sources of CO_2 (various Δ terms) as listed below:

1. Fossil fuels are entirely devoid of $^{14}CO_2$ and their $\Delta_{ff} = -1000$ ‰.

2. The nuclear emissions are of pure $^{14}CO_2$ and in this formulation Δ_n is the $\Delta^{14}CO_2$ signature that a pure $^{14}CO_2$ sample would have. We calculate it using the activity of pure $^{14}CO_2$ sample in the formulation of $\Delta^{14}CO_2$ as follows:

   $$A_s = \lambda \cdot N_a / m_{^{14}C}, \quad (5)$$

   where $N_a = 6.022 \times 10^{23}\,\mathrm{mol}^{-1}$ is the Avogadro constant, $\lambda = 3.8534 \times 10^{-12}$ Bq is the decay rate of ^{14}C and $m_{^{14}C} = 14.0\,\mathrm{g\,mol}^{-1}$ is the molar mass of the isotope. In a sample of a pure $^{14}CO_2$ there is no fractionation and the calculation of $\Delta^{14}CO_2$ (Stuiver and Polach, 1977; Mook and van der Plicht, 1999) can be simplified to the ratio between the activity of the sample and activity of the referenced standard $A_{ABS} = 0.226\,\mathrm{Bq\,g\,C}^{-1}$ (Mook and van der Plicht, 1999):

   $$\Delta_n = A_s / A_{ABS} \cdot 1000\,[‰] \quad (6)$$

   The resulting $\Delta_n \approx 0.7 \times 10^{15}$ [‰] is much higher than any of the other Δ signatures, but this is balanced by the concentrations of the $^{14}CO_2$, which are only a very small fraction ($\sim 10^{-12}$) of the observed CO_2 concentrations.

3. Finally, we use Δ_{bg} from monthly observed $\Delta^{14}CO_2$ at the high alpine station Jungfraujoch (3580 m a.s.l., Switzerland) (Levin et al., 2010), which is considered representative for European $\Delta^{14}CO_2$ background. These are shown in red on Fig. 3a.

We note that the choice of background can be crucial for the estimation of Δ_{obs} and consequently for the recalculation of CO_{2ff}. Local influences captured in the background might modify the seasonality of the derived Δ_{obs} and result in biases when applied to observations from other locations. These influences include local fossil fuel or nuclear signals, biospheric enrichment or modified vertical mixing during parts of the year (Turnbull et al., 2009b).

The transport and resulting spatiotemporal gradients in total CO_2 and $^{14}CO_2$ over Europe are simulated with WRF-CHEM model, described next.

2.2 WRF-CHEM

For our simulation with WRF-Chem (version 3.2.1) (Skamarock et al., 2008) we use meteorological fields from the National Centers for Environmental Prediction Final (FNL) Operational Global Analyses (NCEP, US National Centers for Environmental Prediction, 2011) at $1^\circ \times 1^\circ$ for lateral meteorological boundary conditions, which are updated every 6 h. We model the atmospheric transport and weather for the period between April and September 2008 including. We use three domains with horizontal resolution of 36, 12 and 4 km and, respectively, 60×62, 109×100 and 91×109 grid points, centered over Western Europe and the Netherlands, as shown in Fig. 1. Our vertical resolution includes 27 pressure levels, 18 of which are in the lower 2 km of the troposphere, and the time step used is 180 s in the outer domain. Important physics schemes used are the Mellor-Yamada Nakanishi and Niino (MYNN2.5) boundary layer scheme (Nakanishi and Niino, 2006), the Rapid Radiation Transfer Model (RRTM) as our longwave radiation scheme (Mlawer et al., 1997), and the Dudhia shortwave radiation scheme (Dudhia, 1989). We use the Unified Noah Land-Surface Model (Ek et al., 2003) as our surface physics scheme and additionally use time-varying surface conditions, which we update every 6 h.

We use separate passive tracers for the different CO_2 terms in Eq. (4). We prescribe our initial and lateral boundary conditions for the background CO_2, while the biospheric uptake, respiration, fossil fuel CO_2 and nuclear $^{14}CO_2$ are implemented with surface fluxes only, which are prescribed and provided to the model every hour. Once CO_2 leaves our outer domain it will not re-enter it again. This setup reflects our interest in the recent influence of the biosphere and anthropogenic emissions. For this reason we will avoid using direct results from the outer domain, and instead use only the nested domains, where boundary conditions for all tracers are provided through their respective parent domain.

The background (CO_{2bg}) initial and boundary conditions are implemented using 3-D mole fraction output from CarbonTracker (Peters et al., 2010) for 2008 at $1^\circ \times 1^\circ$ resolution and interpolated vertically from 34 to 27 levels using the pressure fields. The CO_2 lateral boundary conditions are added to the standard meteorological boundary conditions and also updated every 6 h.

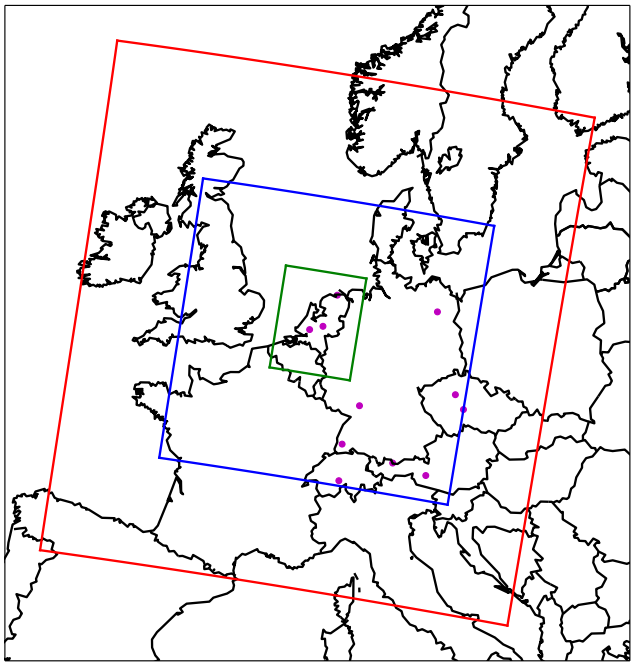

Figure 1. The location of modeled domains. The respective horizontal resolutions are according to the color of the domain boundaries: red – 36 km × 36 km; blue – 12 km × 12 km; green – 4 km × 4 km. The scatter markers indicate the locations of various observational sites used in this study.

Our biospheric fluxes (CO_{2r} and CO_{2p}) are generated using the SiBCASA model (Schaefer et al., 2008; van der Velde et al., 2014), which used meteorological fields from the European Centre for Medium-Range Weather Forecasts (ECMWF). It provides us with monthly averaged gross photosynthetic production (GPP) and terrestrial ecosystem respiration (TER) at 1° × 1° resolution. Due to the coarse resolution of the SiBCASA model, we find land-use categories in the higher resolution map of WRF that are not in the natural land-use map of SiBCASA. To address this issue, we ran 9 simulations with SiBCASA prescribing a single vegetation category, alternating through all the vegetation categories to produce biospheric fluxes for the different land-use categories within the resolution of WRF. For temporal interpolation of the monthly fluxes, we scale the GPP and TER with the instantaneous WRF meteorological variables (temperature at 2 m and shortwave solar radiation) following the method described in Olsen and Randerson (2004).

Anthropogenic (fossil fuel) CO_2 emissions (CO_{2ff}) are from the Institute for Energy Economics and the Rational Use of Energy (IER, Stuttgart, Pregger et al., 2007) at a horizontal resolution of 5 (geographical) minutes over Europe in the form of annual emissions at the location and temporal profiles to add variability during different months, weekdays and hours during the day. These are then aggregated to every WRF domain horizontal resolution and updated every hour for the duration of our simulation. The emissions are introduced only at the lowest (surface) level of the model.

Anthropogenic (nuclear) $^{14}CO_2$ emissions ($^{14}CO_{2n}$) are obtained by applying the method described in Graven and Gruber (2011) for the year of 2008. We used information from the International Atomic Energy Agency Power Reactor Information System (IAEA PRIS, available online at http://www.iaea.org/pris) for the energy production of the nuclear reactors in our domain and reported $^{14}CO_2$ discharges for the spent fuel reprocessing sites (van der Stricht and Janssens, 2010). The data is available only on annual scale and once converted from energy production to emissions of $^{14}CO_2$, these are scaled down to hourly emissions, assuming continuous and constant emission during the year. This is likely true when the nuclear reactors are operating, however, in reality regular maintenance and temporary shutdowns of individual reactors would result in periods of weeks and sometimes months of lower energy production and subsequently lower $^{14}CO_2$ discharge. We will further comment on these assumptions in our Discussion (Sect. 4).

2.3 Integrated $\Delta^{14}CO_2$ air and plant samples

Integrated $\Delta^{14}CO_2$ samples ($\Delta_{absorption}$), where the sampling rate is usually constant (e.g. in various CO_2 absorption setups), are represented with the concentration-weighed time-average $\Delta^{14}CO_2$ signature for the period and height of sampling, as seen in Eq. (7). When actual sampling is restricted to specific wind conditions or times-of-day, we include this in our model sampling scheme as well.

$$\Delta_{absorption} = \sum_t \Delta^t_{obs} \frac{CO^t_{2obs}}{\sum_t CO^t_{2obs}} \quad (7)$$

Plant samples (Δ_{plant}) integrate the atmospheric $\Delta^{14}CO_2$ signature with CO_2 assimilation rate which varies depending on various meteorological and phenological factors. Photosynthetic uptake and the allocation of the assimilated CO_2 in the different plant parts strongly depend on the weather conditions and plant development. To simulate such samples we use WRF meteorological fields in the crop growth model SUCROS2 (van Laar et al., 1997) and use the modeled daily growth increment as a weighting function (averaging kernel) on the daytime atmospheric $\Delta^{14}CO_2$ signatures (Bozhinova et al., 2013). For each location we use the same sowing date and the model simulates the crop development until it reaches flowering, when we calculate Δ_{plant}. More explicitly these integrated sample signatures are calculated as follows:

$$\Delta_{plant} = \sum_t \Delta^t_{obs} \frac{X_t}{\sum_t X_t}, \quad (8)$$

where X_t is the growth increment at time t, which in the case of SUCROS2 simulation is the dry matter weight increment at day t.

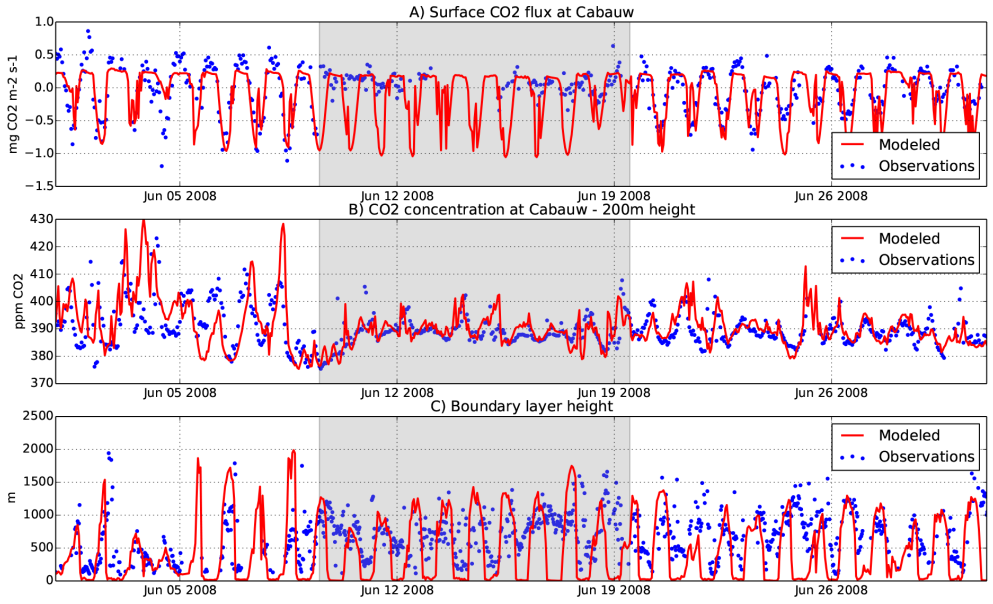

Figure 2. Comparison between modeled and observed CO_2 fluxes, concentrations and boundary layer height for the location of Cabauw for one month in the simulated season. Performance is usually better on clear days as compared to cloudy ones, as indicated in the graph with the gray background.

3 Results

3.1 Model evaluation – how realistic are our CO_2 and $\Delta^{14}CO_2$ simulations?

The meteorological conditions for 2008 that were simulated by WRF and used for the plant growth simulation in SUCROS2 were previously assessed in Bozhinova et al. (2013). Here we assess the model performance compared to observed CO_2 fluxes, CO_2 mole fractions, and boundary layer heights. Figure 2 shows this comparison at the observational tower of Cabauw, the Netherlands (data available at http://www.cesar-observatory.nl). The simulated net CO_2 flux (NEE) compares well to observations with a root-mean squared deviation (RMSD) of $0.26\,\mathrm{mg\,CO_2\,m^{-1}\,s^{-1}}$ and correlation coefficient (r) for the entire period of 0.70, which is even higher in clear days. Overestimates of NEE occur during cloudy conditions, which are notoriously difficult to represent in many mesoscale models. The CO_2 mole fractions compare well to observations (Vermeulen et al., 2011) and overall model performance is similar to other studies for the region (Tolk et al., 2009; Meesters et al., 2012). Similar to Steeneveld et al. (2008), Tolk et al. (2009), Ahmadov et al. (2009) the night-time stable boundary layer poses a challenge to the model. Note that the skill at modeling the boundary layer height can be of a particular importance for the correct simulation of the CO_2 budget, as it controls the diurnal evolution of the CO_2 mole fractions (Vilà-Guerau de Arellano et al., 2004; Pino et al., 2012). Thus, we have included this comparison in the last panel of Fig. 2. More detailed statistics for this and other stations and observations are listed in Table 1. We show the mean difference between the predicted and observed time series, with the according RMSD, and calculated correlation coefficient and coefficient of determination (Willmott, 1982) for each location. While in Table 1 we show the statistics for the daily time-series, we also evaluated their hourly and daytime-only counterparts and the differences between each. Overall, our comparison shows that although the model overestimates the night-time CO_2 concentrations, it captures the observed daytime CO_2 mole fractions features and their variability on scales of hours to days satisfactorily over the full period simulated for Cabauw.

We next analyze the results for the $\Delta^{14}CO_2$ signature corresponding to these CO_2 mole fractions to evaluate our skill at modeling the large scale $^{14}CO_2$ over Europe. Figure 3 shows the comparison between integrated (monthly, bi-weekly or weekly) samples and their modeled counterparts for six measurement sites – Jungfraujoch, Switzerland, Heidelberg and Schauinsland, Germany (Institut für Umweltphysik, University of Heidelberg, Germany, Levin et al., 2013), Prague-Bulovka and Kosetice, Czech Republic (Academy of Sciences of the Czech Republic, Svetlik et al., 2010) and Lutjewad, the Netherlands (Centre for Isotope Research, University of Groningen, The Netherlands, unpublished data for the monthly integrated samples, south sector data was previously used in van der Laan et al., 2010). Complementary statistics are included in Table 1. For the high-altitude locations of Jungfraujoch and Schauinsland the model topography differed significantly from the altitude of the observational site. Similar to the procedure

Table 1. The observational sites with data used in this study and statistics for the daily concentrations of CO_2 and CO_{2ff} estimated from CO observations, hourly flux CO_2 and monthly integrated $\Delta^{14}CO_2$ observations as compared with modeled results. Here $\overline{\text{Pi–Oi}}$ represents the mean model-data difference and $\sigma_{\text{Pi–Oi}}$ is the spread of this difference. Both expressions carry the units described in the header of each section. r and d are respectively the Pearson's coefficient of correlation and the coefficient of determination. n is the number of members used in the statistical analysis.

Site	Latitude [° N]	Longitude [° E]	Elevation [m]	Altitude [m]	Owner	Provider	$\overline{\text{Pi–Oi}}$	$\sigma_{\text{Pi–Oi}}$	r	d	n
CO_2 concentration [ppm]											
Cabauw, NL	51.97	4.93	0.7	20	ECN, NL[a]	CarboEurope IP[b]	5.58	8.19	0.64	0.72	185
Cabauw, NL	51.97	4.93	0.7	60	ECN, NL	CarboEurope IP	3.69	6.37	0.65	0.74	185
Cabauw, NL	51.97	4.93	0.7	120	ECN, NL	CarboEurope IP	2.76	5.48	0.67	0.77	185
Cabauw, NL	51.97	4.93	0.7	200	ECN, NL	CarboEurope IP	1.40	4.50	0.74	0.84	185
Heidelberg, DE	49.42	8.67	116	30	IUP-UHEI, DE[c]	CarboEurope IP	4.29	7.31	0.69	0.77	185
Loobos, NL	52.17	5.74	25	24.5	Alterra-WUR, NL[d]	CarboEurope IP	3.82	6.90	0.59	0.71	185
Lutjewad, NL	53.40	6.36	3	60	CIO-RUG, NL[e]	CIO-RUG, NL	−0.60	7.43	0.53	0.73	167
Neuglobsow, DE	53.17	13.03	65	–	UBA, DE[f]	WDCGG[g]	−2.31	8.62	0.58	0.74	185
Schauinsland, DE – 5 min	47.92	7.92	1200	7	UBA, DE	WDCGG	0.20	4.13	0.81	0.89	153
Schauinsland, DE – conti	47.92	7.92	1200	7	UBA, DE	WDCGG	0.17	3.59	0.85	0.92	177
Sonnblick, AT	47.05	12.95	3106	–	EEA, AT[h]	WDCGG	1.57	2.74	0.86	0.88	185
Zugspitze, DE	47.42	10.98	2656	–	UBA, DE	WDCGG	0.79	3.07	0.82	0.88	161
Estimated fossil fuel CO_2 concentration [ppm]											
Lutjewad, NL – CO_{2ff}	53.40	6.36	3	60	CIO-RUG, NL	CIO-RUG, NL	−3.29	3.64	0.66	0.69	166
CO_2 surface flux [mg $CO_2\,m^{-2}\,s^{-1}$]											
Cabauw, NL	51.97	4.93	0.7	1	KNMI, NL[i]	CESAR[j]	−0.01	0.26	0.70	0.83	2662
$\Delta^{14}CO_2$ integrated sample [‰]											
Heidelberg, DE – weekly	49.42	8.67	116	30	IUP-UHEI, DE	IUP-UHEI, DE	−3.28	3.05	0.82	0.82	26
Jungfraujoch, CH	46.55	8.00	3450	5	IUP-UHEI, DE	IUP-UHEI, DE	1.05	1.61	0.71	0.74	6
Kosetice, CZ	49.58	15.08	534	3.5	NPI AS CR[k]	NPI AS CR	−2.44	6.78	0.07	0.26	6
Lutjewad, NL	53.40	6.36	3	60	CIO-RUG, NL	CIO-RUG, NL	8.82	5.16	−0.87	0.12	6
Lutjewad, NL – south	53.40	6.36	3	60	CIO-RUG, NL	CIO-RUG, NL	0.16	6.79	0.39	0.63	12
Prague-Bulovka, CZ	50.12	14.45	266	8	NPI AS CR	NPI AS CR	−5.23	3.88	0.95	0.77	6
Schauinsland, DE	47.92	7.92	1200	7	IUP-UHEI, DE	IUP-UHEI, DE	−1.89	1.83	0.74	0.75	6

[a] ECN – Energy Research Center of the Netherlands, the Netherlands; contact person – Alex Vermeulen, a.vermeulen@ecn.nl
[b] CarboEuropeIP – CarboEurope Integrated Project; http://www.carboeurope.org
[c] IUP-UHEI – Institute of Environmental Physics, University of Heidelberg, Germany; contact person – Ingeborg Levin, Ingeborg.Levin@iup.uni-heidelberg.de
[d] Alterra-WUR – Alterra, Wageningen University, the Netherlands; contact person – Eddy Moors, eddy.moors@wur.nl
[e] CIO-RUG – Center for Isotope Research, University of Groningen, the Netherlands; contact person – Harro Meijer, H.A.J.Meijer@rug.nl
[f] UBA, DE – Federal Environmental Agency, Germany; contact person – Karin Uhse, karin.uhse@uba.de
[g] WDCGG – World Data Center for Greenhouse Gases; http://ds.data.jma.go.jp/gmd/wdcgg/
[h] EEA, AT – Environmental Agency Austria, Austria; contact person – Marina Fröhlich, marina.froehlich@umweltbundesamt.at
[i] KNMI – Royal Netherlands Meteorological Institute, the Netherlands; contact person – Fred Bosveld, Fred.Bosveld@knmi.nl
[j] CESAR – Cabauw Experimental Site for Atmospheric Research, the Netherlands; http://www.cesar-observatory.nl
[k] NPI AS CR – Nuclear Physics Institute, Academy of Sciences of the Czech Republic, Czech Republic; contact person – Ivo Svetlik, svetlik@ujf.cas.cz

described in Turnbull et al. (2009b) we sampled a model layer in the free troposphere instead of at the modeled surface to better represent the observations. At all other sites we sample the pressure-weighted signature of the boundary layer, applying a minimum boundary layer height of 350 m during the night to avoid sampling too low surface signatures in a too stable nighttime boundary layer. The comparison shows we capture reasonably well the seasonal cycle for most sites, however the model generally underestimates the $\Delta^{14}CO_2$. This is partly caused by the omitted biospheric disequilibrium term, which accounts on average for up to 1.5 ‰ at these latitudes. Additional bias could be introduced through our choice of background site. In their study, Turnbull et al. (2009b) showed that the signature of free tropospheric air in the northern-hemispheric mid-latitudes can vary within 3 ‰ and additionally the signatures at mountain background sites (as Jungfraujoch) are slightly influenced by local fossil fuel emissions.

In the lowest left panel of Fig. 3 we show the comparison for Heidelberg, where observations are collected as weekly night-time (between 19:00 and 07:00 local time) integrated samples. On higher temporal resolution our model estimates reproduce the temporal variations of the observations well. Still, the already discussed underestimation in $\Delta^{14}CO_2$ is also present at this site, which is located near a large urban area with considerable fossil fuel emissions. During the period from May to August, this underestimation is on average 5 ‰ in the model (~ 1.8 ppm of fossil fuel CO_2). In the lowest right panel of Fig. 3 we show the comparison between the observed and modeled signatures at Lutjewad for the wind-specific measurements at this site in addition to the observed monthly samples that were continuously integrated. The monthly $\Delta^{14}CO_2$ observations for 2008 from this location show atypical seasonality with a lack of the expected summer maximum, and 10 to 20 ‰ lower $\Delta^{14}CO_2$ than the observations in Jungfraujoch and Schauinsland in that year. Although this suggests a large fossil fuel CO_2 signal for 2008, we could not find further evidence of this in the rest of the Lutjewad observational record (CO, CO_2), nor in the selected southerly wind sector data (van der Laan

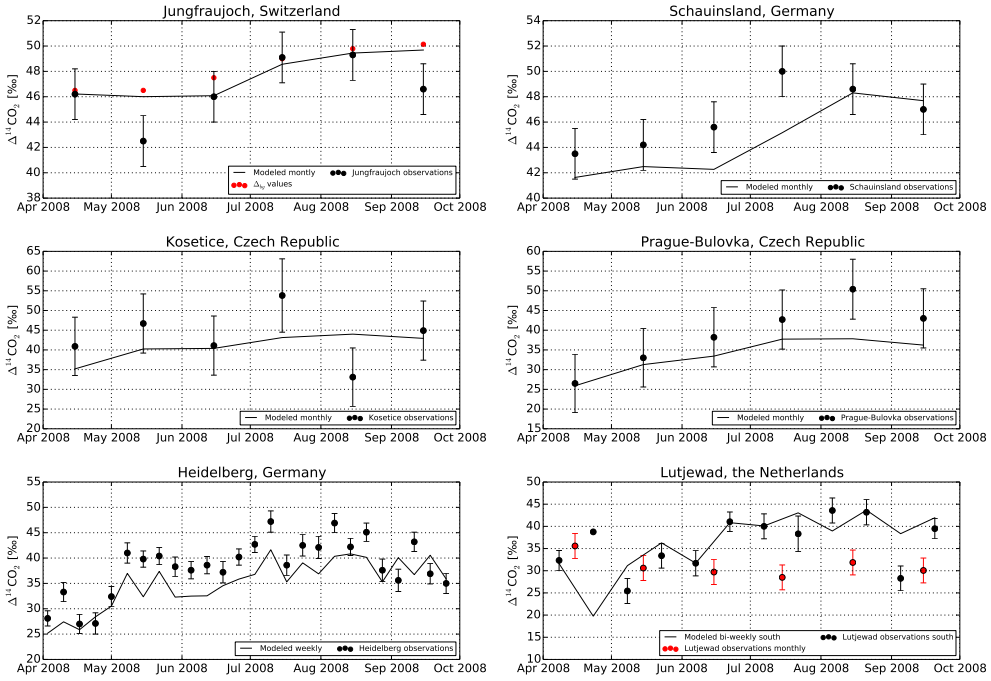

Figure 3. Comparison between observed and modeled atmospheric $\Delta^{14}CO_2$ integrated samples for six observational sites. Red circles in the Jungfraujoch graph show the monthly fit used as the signature of the background CO_2 (Δ_{bg}) in our calculations. Observations are monthly continuously integrated samples at Jungfraujoch, Schauinsland, Kosetice, and Prague. At Heidelberg the weekly samples integrate only during the night-time. At Lutjewad the bi-weekly samples only integrate during periods of southerly winds, and the monthly integral over all sectors (discussed in the main text) is shown in red.

et al., 2010), which our model matches rather well. Since the measurements themselves seem valid, this feature in the continuous monthly Lutjewad $\Delta^{14}CO_2$ data remains unexplained. We will however take a closer look at the temporal variability of the different $\Delta^{14}CO_2$ components and the general model performance at Lutjewad for the more accurately simulated southerly wind sector.

Figure 4 shows the 6-month hourly comparison of simulated and observed CO_2 and fossil derived CO_2 for Lutjewad. The latter is derived from ^{14}C-corrected high-resolution CO observations (van der Laan et al., 2010). Statistics for the comparison are also shown in Table 1. The fossil fuel signal dominates over any variability in the background, clearly defining periods with enhanced transport of fossil fuel CO_2 to the location (late April, start of May, start of July, start of August) as compared to less polluted air transported from the North Sea (mid-May, mid-June). The larger mismatch in particular periods (second half of April, start of May) can be attributed to the specific way the CO observations are calibrated using the 3-year fit of the ^{14}C-CO ratio at the site. While this would ensure that on an annual scale the actual ^{14}C-CO relation is reached, on the bi-weekly scale of the ^{14}C observations this sometimes results underestimation of the ^{14}C-CO ratio compared to the observed values and consequently overestimation of the estimated fossil fuel CO_2. For more information, see van der Laan et al. (2010).

In the last panels we see this influence on the resulting $\Delta^{14}CO_2$ signature and especially its high temporal variability that is not captured in the typically integrated monthly samples. Note that even though station Lutjewad is far away from nuclear emission sources, the signal from nuclear activity (shown in the last panel) can sometimes be of the same order of magnitude as the fossil fuel signal. This shows that it is important to evaluate the nuclear influence at every measurement site using a model like presented here, as it will contribute to the uncertainty in the recalculation of fossil fuel CO_2.

3.2 Fossil fuel vs. nuclear emissions influence on $\Delta^{14}CO_2$

The lowest $\Delta^{14}CO_2$ values in the domain are modeled in the regions with high fossil fuel emission in Germany (the Ruhrgebiet), and the highest $\Delta^{14}CO_2$ is near the large emitting sites in western France and UK. This pattern can be clearly seen in Fig. 5a–c where results averaged over the lower 1200 m of the atmosphere over the full 6 months are shown. Note that the nuclear enrichment reaches much higher amplitude than the opposite effect by the fossil CO_2, but its influence on the atmospheric $\Delta^{14}CO_2$ is usually restricted to the vicinity of the average nuclear power plant reactors. The influence is more pronounced in the western

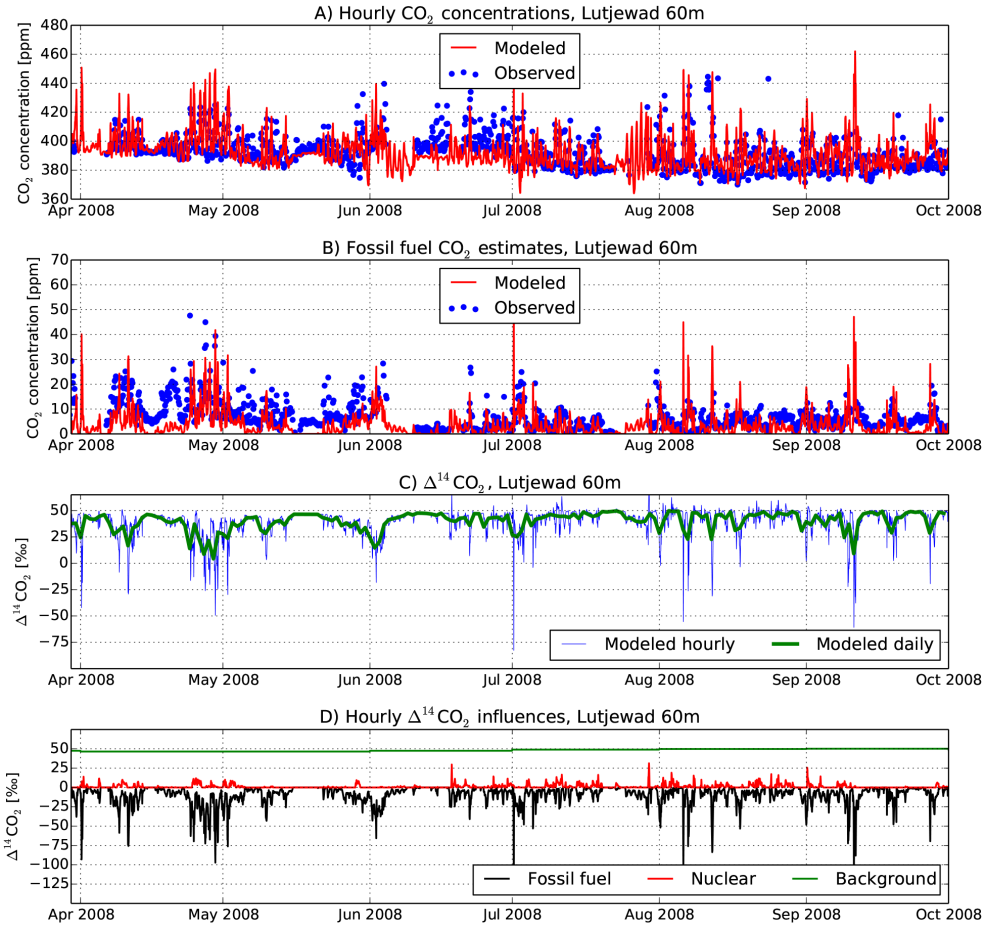

Figure 4. 6 months of hourly results for Lutjewad at 60 m height. Comparison between observed and modeled **(a)** CO_2 concentrations, **(b)** CO_{2ff} concentrations **(c)** atmospheric $\Delta^{14}CO_2$ and **(d)** the contribution of different compounds for the resulting $\Delta^{14}CO_2$. The transport of air that is enriched in fossil fuel CO_2 is directly connected to the variations in the $\Delta^{14}CO_2$ signal at the location, but these are not captured by current observations due to their low temporal resolution.

part of our domain, where it captures the influence from the spent fuel reprocessing plant in La Hague (France) and several newer generation nuclear reactors in the UK. Even then, the influence of the nuclear enrichment averaged over 6 months is typically about 1 to 6 ‰ in areas that are not in direct vicinity of the sources. As a comparison, the fossil fuel influence in our domain on the same temporal and spatial scale is mostly between −3 and −15 ‰ outside the very polluted area of the Ruhrgebiet, Germany.

As the nuclear enrichment will (partially) mask the effect of fossil fuel CO_2 on the atmospheric $\Delta^{14}CO_2$, we show in Fig. 5d the average 6-month ratio of the influences due to nuclear and fossil fuel sources in our domain. Again, in most of the eastern and central parts of our domain the nuclear influence is less than 10 % the fossil fuel influence. This differs from the western part of our domain, where the ratio varies between 3 times smaller to about the same magnitude as the fossil fuel contribution and even to a more than 5 times larger influence in the area around the nuclear sources. The area affected depends on the strength of the source, and in our case the influence of most water-cooled reactors rarely exceeds the grid cell of the source, while for the gas-cooled reactors the influence can be seen up to 50 km distance. These findings are consistent with Graven and Gruber (2011). The magnitude of the enrichment and size of the area influenced are both highly variable and strongly dependent on the atmospheric transport. As a result, in months with dominant easterly winds the nuclear enrichment has a minimum effect in our domain, as most of the nuclear emissions are transported towards the Atlantic ocean and out of our area of interest. However, in months with dominant westerly winds, which is the prevailing wind direction, the nuclear $^{14}CO_2$ spreads widely over the domain.

Graven and Gruber (2011) evaluated the uncertainty of the emission factors reported in previous literature and estimated mean values with associated 70 % confidence interval. While for our main results we used the estimated mean emission factors for a 2-month period we separately simulated the

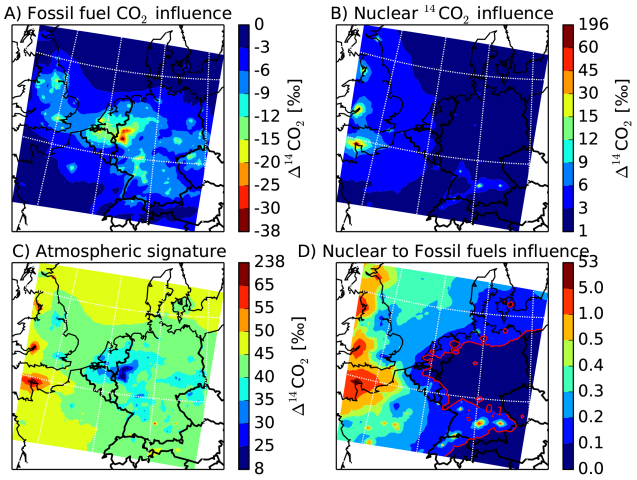

Figure 5. Spatial distribution for the 6-month averaged **(a)** fossil fuel CO_2 emissions influence, **(b)** nuclear $^{14}CO_2$ emissions influence, **(c)** resulting $\Delta^{14}CO_2$ signature in the atmosphere and **(d)** the ratio between the nuclear and fossil fuel influences on the atmospheric signature, all averaged over the lower 1200 m of the atmosphere. While the largest influence over Europe is from fossil fuel CO_2, the effect of the nuclear emissions of $^{14}CO_2$ can be of comparable magnitude for large areas in France and UK.

70 % confidence interval of the emission factors ("low estimate" and "high estimate" runs). In Fig. 6 we show these results as the absolute difference when compared to the mean run. While our largest source of nuclear emissions – located in La Hague, France, has directly reported emissions of $^{14}CO_2$ and is thus not subject to uncertainty in the emission factors, considerably higher or lower $^{14}CO_2$ signatures could be associated with the nuclear estimates in the United Kingdom, southern Germany and central France.

For sites located in northern and central France, southern Germany and the UK the nuclear enrichment means that corrections are needed that account for the nuclear influence in the observed $\Delta^{14}CO_2$ before estimating the fossil fuel influence. As an illustration, we show in Fig. 7 the influence of the different anthropogenic emissions for three locations with different characteristics in our domain: Cambridge (UK), Cabauw (the Netherlands) and Kosetice (Czech Republic). The locations were chosen to be in rural or agricultural areas, without large local CO_2 emissions. As seen in Fig. 7, the western part of our domain (represented by Cambridge) has an equal influence from fossil fuel and nuclear emissions; the center (represented by Cabauw) experiences some events with relatively high nuclear emissions influence, but is influenced mostly by the very high fossil fuel emissions in this region (on average about 3 times higher than in Cambridge). In the east (represented by Kosetice) there is no significant signal of influence of nuclear emissions, but the influence of fossil fuel emissions is also considerably lower.

3.3 $\Delta^{14}CO_2$ plant vs. atmospheric samples

In our previous work (Bozhinova et al., 2013) we described a method to model the $\Delta^{14}CO_2$ in plant samples as the first step in quantifying the differences between such samples and integrated atmospheric samples. Here we build on this work by calculating the plant signature resulting from uptake of spatially and temporally variable atmospheric $\Delta^{14}CO_2$. The results for modeled samples from maize leaves at flowering, are shown in Fig. 8. Clearly, spatial gradients in $\Delta^{14}CO_2$ in plants are sizeable compared to the measurement precision of approximately 2 ‰. The regions with high influence from anthropogenic emissions from Fig. 5, namely the Ruhrgebiet in western Germany and the Benelux are also visible in the modeled plant signature, and so are some hot spots around larger european cities, like Frankfurt, Paris, London and others. It is important to point out that in addition to fossil fuel and nuclear gradients, plants develop at a different rate in different parts of the domain, and even the different parts of a plant (roots, stems, leaves, fruits) grow during different time periods.

The plant-sampled $\Delta^{14}CO_2$ includes the effect of the covariance between the atmospheric $\Delta^{14}CO_2$ variability and the variability in the assimilation of CO_2 in the plant during growth, which is absent in traditional integrated samples where the absorption of CO_2 is based on constant flow rate through an alkaline solution and thus only varies with the CO_2 concentration present in the flow (Hsueh et al., 2007). In Fig. 9 (left) we show this effect of the plant growth on the resulting plant $\Delta^{14}CO_2$ signature when comparing the resulting plant signature with the daytime atmospheric average we provide to our crop model. We should stress, that this is the magnitude of the error one should expect if the plant-sampled $\Delta^{14}CO_2$ is assumed equal to the atmospheric mean $\Delta^{14}CO_2$ for the growing period of the plant. For many parts of Europe in our simulated period this error is approaching the measurement precision of the $\Delta^{14}CO_2$ analysis (of approximately ± 2 ‰). In the region located between the areas with high fossil fuel and large nuclear emitters, however, the magnitude of the error can be several times larger. This is likely due to the absorption of some very high signature values in periods when the wind direction is directly from the nuclear source. Actual plant samples, taken during different period than the one investigated here (namely 2010–2012), will be used to further investigate these signatures in a follow-up publication.

We also evaluated the bias that would be introduced if the nuclear influence is not included in the modeling of the plant samples. We show this on Fig. 9 (right) as the difference between the plant signatures when the nuclear influence is included or excluded from the simulation. For the continental part of our domain this bias mostly stays within 0–4 ‰, while in the United Kingdom it ranges from 2–8 ‰ and higher. This suggests that also when interpreting plant samples, the ability

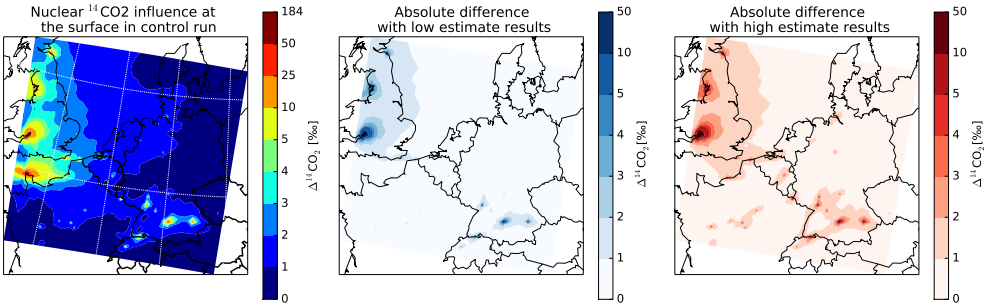

Figure 6. Spatial distribution for the uncertainty in the nuclear $^{14}CO_2$ influence simulated for August and September, due to the uncertainty in the emission factors associated with different reactor types. (Left) The nuclear influence modeled with the central estimate of the reactor emission factors; (middle) the absolute difference between the lower estimate and central estimate; (right) the absolute difference between the higher estimate and the central estimate. Low and high estimates refer to the 70 % confidence interval for the emission factors.

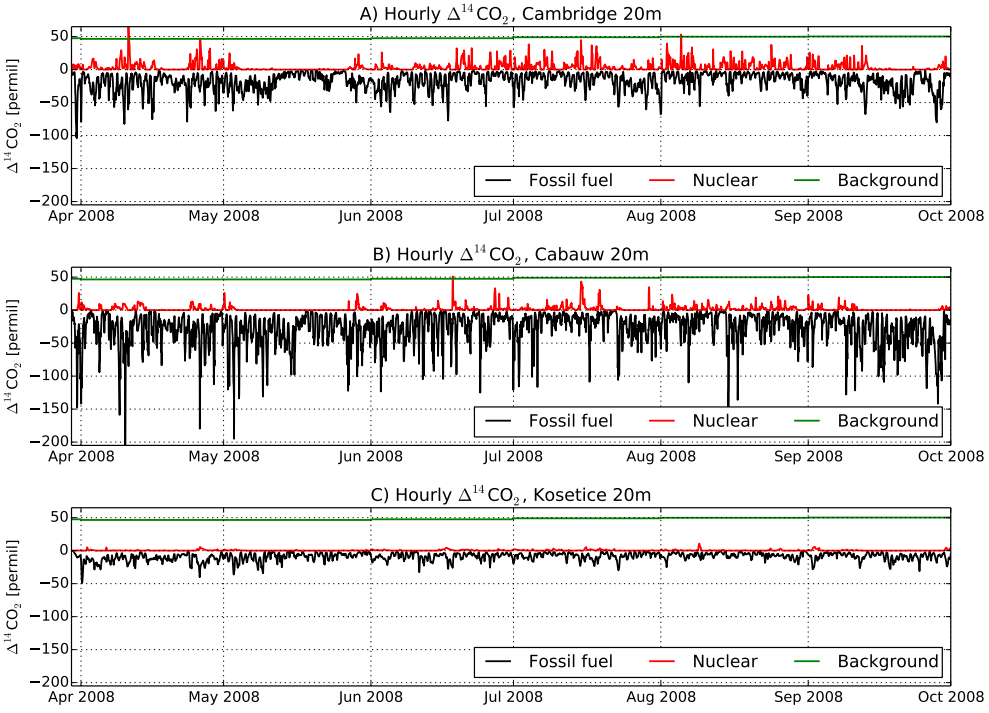

Figure 7. Time series for the relative importance of nuclear vs. fossil fuel influence on the resulting atmospheric $\Delta^{14}CO_2$ for three locations in our domain – near Cambridge (UK), Cabauw (the Netherlands) and Kosetice (Czech Republic).

to correctly account for nuclear influences such as through a modeling system could be important.

3.4 Direct estimation of the fossil fuel CO_2 emissions

While the entire emission map of Europe might be difficult to verify, most of the fossil fuel CO_2 emissions are produced at only a number of locations. For instance, 10 % of all emissions in our domain come from only 30 grid cells and more than half of these are located in densely populated cities or urban conglomerations. This might provide an opportunity for a better fossil fuel estimate of the highest emitting regions in Europe even when only selected locations are visited in a plant sampling campaign. One could for instance assume that the $\Delta^{14}CO_2$ signatures in plants in these high-emission areas directly reflect the local anthropogenic sources, and a straightforward determination of their $^{14}CO_2$ signature would suffice to estimate emissions using a simple box-model approach. We show in the following analysis that this simplification can lead to large errors though, and a more complete modeling framework like ours is needed for a proper interpretation of $\Delta^{14}CO_2$.

In our modeling framework, we know the exact emissions we prescribe in each grid box as well as the resulting atmospheric $\Delta^{14}CO_2$ signatures. If we take the anthropogenic

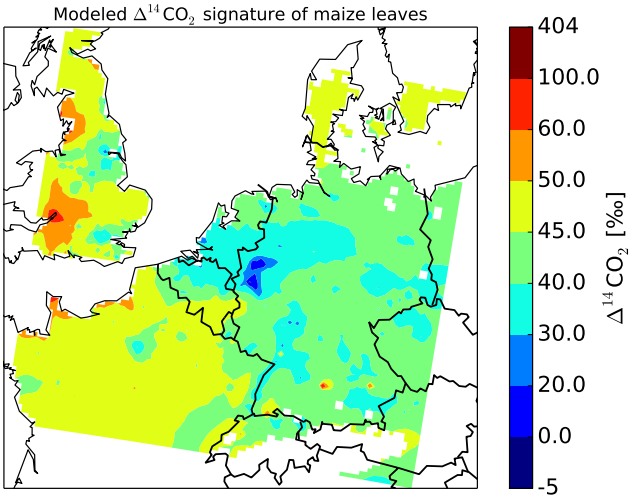

Figure 8. Modeled absolute $\Delta^{14}CO_2$ signature of maize leaves at flowering. Both the highly industrialized areas in Germany, where the atmospheric $\Delta^{14}CO_2$ is lower than the background, and the enriched areas near the big nuclear sources in France and UK are visible also in the plants. Even on this resolution we see in the plant signature the hot spots around Paris, London, Frankfurt, and many other big cities.

emissions over a 60 km × 60 km area around 25 large European cities, mix them through a 500 m deep boundary layer (typical 24 h average for our domain), and assume the air to have a residence time of 3.3 h (corresponding to a typical wind speed of 5 ms^{-1} through a 60 km domain), we can make a simple estimate of the resulting $\Delta^{14}CO_2$ signature relative to the background from Jungfraujoch. This box-model estimate is shown in Fig. 10 as the continuous straight line, in which the downward slope with increasing emissions is controlled mostly by the assumed residence time and the prescribed boundary layer height.

If we compare this linear relationship with the simulated $\Delta^{14}CO_2$ signatures over these cities simulated with the full model developed in this paper (including its detailed horizontal advection, vertical mixing, and nuclear influence), one can see the large variability and substantial bias one would incur using the simple box-model approach. Up to 8 ‰ differences from this line would be found for Paris and Cologne, while the nuclear influence would lift Birmingham plant samples back toward the Jungfraujoch background $\Delta^{14}CO_2$ despite its emissions being similar to Berlin. Even if the full model-derived slope of approximately −4.85 ‰ per 10 000 mol km^{-2} h^{-1} could be reproduced with the box-model, the coefficient of determination (R^2) would be just over 0.7, meaning that close to 30 % of the spatial variance in emissions across Western Europe will not be captured in the simple approach. We therefore caution strongly against a simplified quantitative interpretation of $\Delta^{14}CO_2$ signatures, both in plants and in the atmosphere.

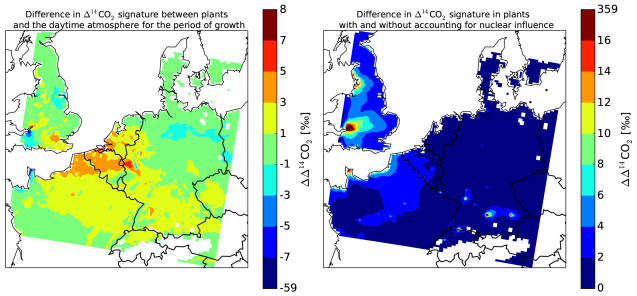

Figure 9. Difference between $\Delta^{14}CO_2$ modeled in plants and the daytime atmospheric average (left) and between modeled plants with and without taking the nuclear influence into account (right). While the left figure shows the error that should be expected if the plant growth is not taken into account and the plant signature is assumed to be equal to the atmospheric average, the right one shows the error that will be introduced if nuclear emissions of $^{14}CO_2$ are not accounted for in the model simulation.

With a typical $\Delta^{14}CO_2$ single measurement precision of about ±2 ‰ and the full model-derived slope given above, we can tentatively estimate that even a perfect modeling framework will have a remaining uncertainty of 4000 mol km^{-2} h^{-1} for area-average emissions in these top-25 emitters over Europe. This is quite substantial (20–50 %) for most of them, with the possible exception of the cities in the German Ruhr area (5–15 %). We therefore see an important role for a monitoring program of $\Delta^{14}CO_2$ signatures in which emissions from all major sources are captured in multiple samples from multiple locations to minimize dependence on single observations and single atmospheric transport conditions. A modeling framework that can capture the specific characteristics of the regional atmospheric transport, fossil fuel emissions, and nuclear contributions like the one presented here would bring added value to the interpretation of such data.

4 Discussion

Our modeling results show that over a significant part of our domain, the nuclear influence on the atmospheric $\Delta^{14}CO_2$ signature will be more than 10 % (ratio = 0.1 on Fig. 5d) of the estimated fossil fuel influence, introducing considerable uncertainty to the method of using $\Delta^{14}CO_2$ to calculate the fossil fuel CO_2 addition to the regional atmosphere. The strongest gradients of $\Delta^{14}CO_2$ in Western Europe are found in the relatively polluted region in western Germany and the Netherlands due to the high population density and large industry sector there, and hence high CO_2 emissions. As was shown for California by Riley et al. (2008), more detailed $^{14}CO_2$ observations in this region can possibly prove useful in lowering the uncertainty of the regional fossil fuel emission estimates. Furthermore, the high fossil-to-nuclear ratio

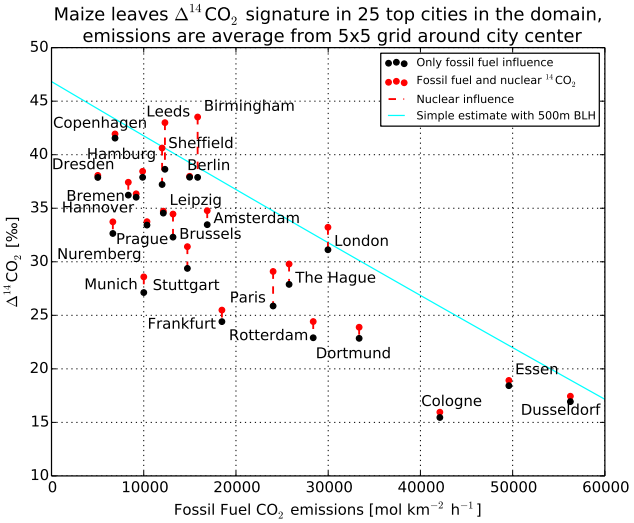

Figure 10. Comparison between the results of the simple box model (see main text) and the modeled maize leaves $\Delta^{14}CO_2$ signature at city center and fossil fuel CO_2 emissions averaged for 5×5 grid around the city center on 12 km horizontal resolution.

ensures that uncertainties arising from nuclear emissions will be at their minimum.

This result relies partly on the underlying emission maps for the anthropogenic (fossil fuel) CO_2 and (nuclear) $^{14}CO_2$ emissions. We should consider various factors that are uncertain or unknown at this point for these emissions (Peylin et al., 2011; Graven and Gruber, 2011) – such as temporal characters, vertical resolution and even small irregularities in the spatial allocation of the emission sources. All our anthropogenic emissions are currently introduced in the lowest (surface) layer of our model, but according to the emission database used (IER, Stuttgart), most of the industrial emission stacks are located on average at 100 to 300 m height. Using this information in our model will likely result in the emitted CO_2 being transported away faster, and result in less local enrichment. This is also true for our nuclear emissions sources, but information on their vertical emission heights is more difficult to find.

For the fossil fuel CO_2 emissions we apply temporal profiles that disaggregate monthly, weekly and diurnal signals from the provided annual emissions. For the nuclear emissions such profiles are unknown and information on their temporal heterogeneity is not publicly available. In this study we consider these emissions as continuous and constant throughout the year. This is a relatively safe assumption for the emissions from nuclear power plants as their $^{14}CO_2$ is a by-product of the normal operation of the reactor. Temporary shutdowns for scheduled maintenance that covers periods of weeks and sometimes months would invalidate this assumed emission pattern. Continuous constant emissions are not likely for reprocessing sites, where the emissions will depend on the type and amount of fuel being reprocessed. Additionally, there is uncertainty if these emissions are released continuously or in a few large venting events, where the venting procedures are moreover likely to be reactor-type dependent. Currently, we lack the information to account for such complications.

When using flask samples for $^{14}CO_2$ measurement nuclear enrichment can relatively easily be recognized. However, in integrated air and plant samples this signal will be averaged over the total sampling period. Depending on weather variability, local fossil fuel CO_2 addition and the proximity to the nuclear sources, the enrichment in $\Delta^{14}CO_2$ can often be within the measurement precision (of approximately ±2 ‰) as we have shown. Thus, integrated samples likely have too low time resolution and sensitivity to attribute nuclear emissions, and areas where this influence is high would profit from flask sampling of $\Delta^{14}CO_2$ in addition to integrated plant sampling. Because plant samples can be used only as complementary observations during particular seasons and depending on the species sampled a dual monitoring approach with flasks and integrated samples seems best. Based on our results, a better characterization of the temporal structure of the nuclear emissions is a prerequisite for any $^{14}CO_2$-based monitoring effort in Europe.

Our study is subject to known uncertainties in atmospheric transport of mesoscale models. An inaccurate simulation of wind speed and direction (Lin and Gerbig, 2005; Gerbig et al., 2008; Ahmadov et al., 2009) or boundary layer height development (Vilà-Guerau de Arellano et al., 2004; Steeneveld et al., 2008; Pino et al., 2012) will affect the transport of emission plumes and resulting mole fractions. Resolving more meso-scale circulations, and improved representation of topography can be particularly advantageous, as they can cause large gradients in CO_2 (de Wekker et al., 2005; van der Molen and Dolman, 2007). While WRF-Chem is used for a variety of atmospheric transport studies (among others: Tie et al., 2009; de Foy et al., 2011; Lee et al., 2011; Stuefer et al., 2013), more general air quality studies have shown that an ensemble of models can forecast air pollution situations more accurately than a single model (Galmarini et al., 2004, 2013). While in our research we focused on the transport of CO_2 and $^{14}CO_2$, other chemically active tracers (e.g. CO, NO_x) that are regularly measured and connected with anthropogenic emissions could be used too. Including ^{222}Rn as an additional tracer can help lowering the uncertainty associated with the vertical mixing in the model and provide correction factors to be applied to the other passive tracers, as shown in van der Laan et al. (2010), Vogel et al. (2013).

Considering future uses of $\Delta^{14}CO_2$ observations as additional constraint on the carbon cycle, we should note that atmospheric inversions currently typically use only afternoon observational data. In that case, plant-sampled $\Delta^{14}CO_2$ observations may provide a better representation of the afternoon atmospheric $\Delta^{14}CO_2$ signals than conventional integrated samples that also absorb CO_2 during the night.

However, the use of plant samples is typically limited to the summertime, which is a period with lower anthropogenic CO_2 emissions, more vertical mixing and larger biospheric fluxes. This will correspond to larger uncertainty in the recalculation of the fossil fuel CO_2 emissions compared to wintertime.

We explored the possibility that a relatively simple box-model can be used to calculate the emissions directly from $\Delta^{14}CO_2$ observations, and showed its inability to capture the variability in $\Delta^{14}CO_2$ signals across 25 European cities. Using such a simple box model has high inherent uncertainty for the reconstructed emissions, a portion of which is a direct consequence of the $\Delta^{14}CO_2$ measurement precision.

Our results suggest that a combination of the available sampling methods should be used when planning a $^{14}CO_2$ observational network for fossil fuel emissions estimates. Integrated air and plant samples alone can provide a longer period observations at a lower cost, but are less useful for evaluation of large nuclear influences in shorter periods. Flask samples are much better suited for this, however their continuous analysis is too costly. A possible compromise could be to obtain flask samples for a limited period alongside integrated samples for new sampling locations. This would already provide information about the possible nuclear enrichment and the wind directions from which it usually occurs. Additionally, while integrated air samples are the current standard for quasi-continuous observations of $^{14}CO_2$, plant samples can be obtained at a much higher spatial resolution without additional infrastructure investment. Their use is however constrained to the sunlit part of the day and generally the summer season, and the exact time and locations where the chosen crop grows.

5 Conclusions

In this work, we demonstrated the ability of our modeling framework to simulate the atmospheric transport of CO_2 and consequently the atmospheric $\Delta^{14}CO_2$ signature in integrated air and plant samples in Western Europe. Based on our results we reach the following conclusions.

1. Simulated spatial gradients of $\Delta^{14}CO_2$ are of measurable size and the 6-month average CO_{2ff} concentrations in the lower 1 km of the atmosphere across Western Europe are between 1 to 18 ppm.

2. Enrichment by $^{14}CO_2$ from nuclear sources can partly mask the Suess effect close to nuclear emissions, particularly in large parts of UK and northwestern France. This is consistent with previous studies (Graven and Gruber, 2011) and we show that in these regions the strength of the nuclear influence can exceed the influence from fossil fuel emissions.

3. The simulated plant $\Delta^{14}CO_2$ signatures show spatial gradients consistent with the simulated atmospheric gradients. Plant growth variability induces differences between the simulated plant and the daytime atmospheric mean for the period of growth, of a magnitude that is mostly within the measurement precision of ± 2 ‰, but can be up to ± 7 ‰ in some areas.

4. Integrated $\Delta^{14}CO_2$ samples from areas outside the immediate enrichment area of nuclear emission sources are not sensitive to occasional advection of enriched air due to their long absorption period. However, to properly account for the nuclear enrichment term on smaller time scales, improvements in temporal profiles of nuclear emissions are needed.

5. New $\Delta^{14}CO_2$ sampling strategies should take advantage of different sampling methods, as their combined use will provide a more comprehensive picture of the atmospheric $\Delta^{14}CO_2$ temporal and spatial distribution.

Acknowledgements. This work is part of project (818.01.019), which is financed by the Netherlands Organisation for Scientific Research (NWO). Further partial support was available by NWO VIDI grant (864.08.012). We acknowledge IER (Stuttgart, Germany) for providing the anthropogenic CO_2 emissions maps, IAEA PRIS for the nuclear reactor information and NCEP and ECMWF for the meteorological data. We thank I. Levin (University of Heidelberg), I. Svetlik (Academy of Sciences, Czech Republic)A. Vermeulen (ECN), S. Palstra and R. Neubert (CIO), E. Moors (Alterra), M. Fröhlich (EAA, Austria), K. Uhse (UBA, Germany) and F. C. Bosveld (KNMI) for providing the observational data used in this study. We further want to thank H. Graven (Imperial College London, UK), N. Gruber (Swiss Federal Institute of Technology, Switzerland), and I. van der Laan-Luijkx and M. Combe (Wageningen University, the Netherlands) for the scientific support and useful comments provided for this manuscript.

Edited by: M. Heimann

References

Ahmadov, R., Gerbig, C., Kretschmer, R., Körner, S., Rödenbeck, C., Bousquet, P., and Ramonet, M.: Comparing high resolution WRF-VPRM simulations and two global CO_2 transport models with coastal tower measurements of CO_2, Biogeosciences, 6, 807–817, doi:10.5194/bg-6-807-2009, 2009.

Anderson, E., Libby, W., Weinhouse, S., Reid, A., Kirshenbaum, A., and Grosse, A.: Natural Radiocarbon from Cosmic Radiation, Phys. Rev., 72, 931–936, doi:10.1103/PhysRev.72.931, 1947.

Bozhinova, D., Combe, M., Palstra, S., Meijer, H., Krol, M., and Peters, W.: The importance of crop growth modeling to interpret the $\Delta^{14}CO_2$ signature of annual plants, Global Biogeochem. Cy., 27, 792–803, doi:10.1002/gbc.20065, 2013.

Ciais, P., Paris, J. D., Marland, G., Peylin, P., Piao, S. L., Levin, I., Pregger, T., Scholz, Y., Friedrich, R., Rivier, L., Houwelling, S., and Schulze, E. D.: The European carbon balance. Part 1: Fossil fuel emissions, Glob. Change Biol., 16, 1395–1408, doi:10.1111/j.1365-2486.2009.02098.x, 2010.

de Foy, B., Burton, S. P., Ferrare, R. A., Hostetler, C. A., Hair, J. W., Wiedinmyer, C., and Molina, L. T.: Aerosol plume transport and transformation in high spectral resolution lidar measurements and WRF-Flexpart simulations during the MILAGRO Field Campaign, Atmos. Chem. Phys., 11, 3543–3563, doi:10.5194/acp-11-3543-2011, 2011.

de Wekker, S. F. J., Steyn, D. G., Fast, J. D., Rotach, M. W., and Zhong, S.: The performance of RAMS in representing the convective boundary layer structure in a very steep valley, Environ. Fluid Mech., 5, 35–62, doi:10.1007/s10652-005-8396-y, 2005.

Djuricin, S., Pataki, D. E., and Xu, X.: A comparison of tracer methods for quantifying CO_2 sources in an urban region, J. Geophys. Res.-Atmos., 115, D11303, doi:10.1029/2009JD012236, 2010.

Dudhia, J.: Numerical study of convection observed during the Winter Monsoon Experiment using a mesoscale two-dimensional model, J. Atmos. Sci., 46, 3077–3107, 1989.

Ek, M., Mitchell, K., Lin, Y., Rogers, E., Grunmann, P., Koren, V., Gayno, G., and Tarpley, J.: Implementation of NOAH land surface model advances in the National Centers for Environmental Prediction operational mesoscale Eta model, J. Geophys. Res.-Atmos., 108, 8851, doi:10.1029/2002JD003296, 2003.

Francey, R., Trudinger, C., van der Schoot, M., Law, R., Krummel, P., Langenfelds, R., Steele, L. P., Allison, C., Stavert, A., Andres, R., and Rodenbeck, C.: Atmospheric verification of anthropogenic CO_2 emission trends, Nature Climatic Change, 3, 520–524, doi:10.1038/nclimate1817, 2013.

Friedlingstein, P., Houghton, R., Marland, G., Hackler, J., Boden, T., Conway, T., Canadell, J., Raupach, M., Ciais, P., and Quéré, C. L.: Update on CO_2 emissions, Nat. Geosci., 3, 811–812, 2010.

Galmarini, S., Bianconi, R., Addis, R., Andronopoulos, S., Astrup, P., Bartzis, J., Bellasio, R., Buckley, R., Champion, H., Chino, M., D'Amours, R., Davakis, E., Eleveld, H., Glaab, H., Manning, A., Mikkelsen, T., Pechinger, U., Polreich, E., Prodanova, M., Slaper, H., Syrakov, D., Terada, H., and Auwera, L. V. D.: Ensemble dispersion forecasting – Part II: Application and evaluation, Atmos. Environ., 38, 4619–4632, 2004.

Galmarini, S., Kioutsioukis, I., and Solazzo, E.: *E pluribus unum*: ensemble air quality predictions, Atmos. Chem. Phys., 13, 7153–7182, doi:10.5194/acp-13-7153-2013, 2013.

Gerbig, C., Körner, S., and Lin, J. C.: Vertical mixing in atmospheric tracer transport models: error characterization and propagation, Atmos. Chem. Phys., 8, 591–602, doi:10.5194/acp-8-591-2008, 2008.

Graven, H. D. and Gruber, N.: Continental-scale enrichment of atmospheric $^{14}CO_2$ from the nuclear power industry: potential impact on the estimation of fossil fuel-derived CO_2, Atmos. Chem. Phys., 11, 12339–12349, doi:10.5194/acp-11-12339-2011, 2011.

Graven, H. D., Guilderson, T. P., and Keeling, R. F.: Observations of radiocarbon in CO_2 at La Jolla, California, USA 1992–2007: Analysis of the long-term trend, J. Geophys. Res.-Atmos., 117, D02302, doi:10.1029/2011JD016533, 2012a.

Graven, H. D., Guilderson, T. P., and Keeling, R. F.: Observations of radiocarbon in CO_2 at seven global sampling sites in the Scripps flask network: Analysis of spatial gradients and seasonal cycles, J. Geophys. Res.-Atmos., 117, D02303, doi:10.1029/2011JD016535, 2012b.

Gurney, K., Mendoza, D., Zhou, Y., Fischer, M., Miller, C., Geethakumar, S., and Can, S. D.: High resolution fossil fuel combustion CO_2 emission fluxes for the United States, Environ. Sci. Technol., 43, 5535–5541, 2009.

Hsueh, D. Y., Krakauer, N. Y., Randerson, J. T., Xu, X., Trumbore, S. E., and Southon, J. R.: Regional patterns of radiocarbon and fossil fuel-derived CO_2 in surface air across North America, Geophys. Res. Lett., 34, L02816, doi:10.1029/2006GL027032, 2007.

Koffi, E. N., Rayner, P. J., Scholze, M., Chevallier, F., and Kaminski, T.: Quantifying the constraint of biospheric process parameters by CO_2 concentration and flux measurement networks through a carbon cycle data assimilation system, Atmos. Chem. Phys., 13, 10555–10572, doi:10.5194/acp-13-10555-2013, 2013.

Kuc, T., Rozanski, K., Zimnoch, M., Necki, J., and Korus, A.: Anthropogenic emissions of CO_2 and CH_4 in an urban environment, Appl. Energ., 75, 193–203, 2003.

Lee, S.-H., Kim, S.-W., Trainer, M., Frost, G. J., McKeen, S. A., Cooper, O. R., Flocke, F., Holloway, J. S., Neuman, J. A., Ryerson, T., Senff, C. J., Swanson, A. L., and Thompson, A. M.: Modeling ozone plumes observed downwind of New York City over the North Atlantic Ocean during the ICARTT field campaign, Atmos. Chem. Phys., 11, 7375–7397, doi:10.5194/acp-11-7375-2011, 2011.

Levin, I. and Hesshaimer, V.: Radiocarbon – a unique tracer of global carbon cycle dynamics, Radiocarbon, 42, 69–80, 2000.

Levin, I. and Karstens, U.: Inferring high-resolution fossil fuel CO_2 records at continental sites from combined $^{14}CO_2$ and CO observations, Tellus B, 59, 245–250, 2007.

Levin, I. and Kromer, B.: Twenty years of atmospheric $^{14}CO_2$ observations at Schauinsland station, Germany, Radiocarbon, 39, 205–218, 1997.

Levin, I. and Rödenbeck, C.: Can the envisaged reductions of fossil fuel CO_2 emissions be detected by atmospheric observations?, Naturwissenschaften, 95, 203–208, 2008.

Levin, I., Munnich, K., and Weiss, W.: The effect of anthropogenic CO_2 and ^{14}C sources on the distribution of ^{14}C in the atmosphere, Radiocarbon, 22, 379–391, 1980.

Levin, I., Schuchard, J., Kromer, B., and Munnich, K. O.: The continental European Suess effect, Radiocarbon, 31, 431–440, 1989.

Levin, I., Kromer, B., Schmidt, M., and Sartorius, H.: A novel approach for independent budgeting of fossil fuel CO_2 over Europe by $^{14}CO_2$ observations, Geophys. Res. Lett, 30, 2194, doi:10.1029/2003GL018477, 2003.

Levin, I., Hammer, S., Kromer, B., and Meinhardt, F.: Radiocarbon observations in atmospheric CO_2: determining fossil fuel CO_2 over Europe using Jungfraujoch observations as background, Sci. Total. Environ., 391, 211–216, 2008.

Levin, I., Naegler, T., Kromer, B., Diehl, M., Francey, R. J., Gomez-Pelaez, A. J., Steele, L. P., Wagenbach, D., Weller, R., and Worthy, D. E.: Observations and modelling of the global distribution and long-term trend of atmospheric $^{14}CO_2$, Tellus B, 62, 26–46, doi:10.1111/j.1600-0889.2009.00446.x, 2010.

Levin, I., Kromer, B., and Hammer, S.: Atmospheric $\Delta^{14}CO_2$ trend in Western European background air from 2000 to 2012, Tellus B, 65, 20092, doi:10.3402/tellusb.v65i0.20092, 2013.

Libby, W.: Atmospheric helium three and radiocarbon from cosmic radiation, Phys. Rev., 671–672, doi:10.1103/PhysRev.69.671.2, 1946.

Lin, J. C. and Gerbig, C.: Accounting for the effect of transport errors on tracer inversions, Geophys. Res. Lett., 32, L01802, doi:10.1029/2004GL021127, 2005.

Lopez, M., Schmidt, M., Delmotte, M., Colomb, A., Gros, V., Janssen, C., Lehman, S. J., Mondelain, D., Perrussel, O., Ramonet, M., Xueref-Remy, I., and Bousquet, P.: CO, NO_x and $^{13}CO_2$ as tracers for fossil fuel CO_2: results from a pilot study in Paris during winter 2010, Atmos. Chem. Phys., 13, 7343–7358, doi:10.5194/acp-13-7343-2013, 2013.

Marland, G.: Uncertainties in Accounting for CO_2 From Fossil Fuels, J. Ind. Ecol., 12, 136–139, doi:10.1111/j.1530-9290.2008.00014.x, 2008.

Marland, G. and Rotty, R.: Carbon dioxide emissions from fossil fuels: a procedure for estimation and results for 1950–1982, Tellus B, 36, 232–261, doi:10.1111/j.1600-0889.1984.tb00245.x, 1984.

McCartney, M., Baxter, M. S., and Scott, E. M.: Carbon-14 discharges from the nuclear fuel cycle: 1. Global effects, J. Environ. Radioactiv., 8, 143–155, 1988a.

McCartney, M., Baxter, M. S., and Scott, E. M.: Carbon-14 discharges from the nuclear fuel cycle: 2. Local effects, J. Environ. Radioactiv., 8, 157–171, 1988b.

Meesters, A., Tolk, L., Peters, W., Hutjes, R., Vellinga, O., Elbers, J., Vermeulen, A., Laan, S. V. D., Neubert, R., Meijer, H., and Dolman, A.: Inverse carbon dioxide flux estimates for the Netherlands, J. Geophys. Res.-Atmos., 117, D20306, doi:10.1029/2012JD017797, 2012.

Meijer, H. A. J., Smid, H., Perez, E., and Keizer, M. G.: Isotopic characterisation of anthropogenic CO_2 emissions using isotopic and radiocarbon analysis, Phys. Chem. Earth, 21, 483–487, doi:10.1016/S0079-1946(97)81146-9, 1996.

Miller, J., Lehman, S., Montzka, S., Sweeney, C., Miller, B., Karion, A., Wolak, C., Dlugokencky, E., Southon, J., Turnbull, J., and Tans, P.: Linking emissions of fossil fuel CO_2 and other anthropogenic trace gases using atmospheric $^{14}CO_2$, J. Geophys. Res.-Atmos., 117, D08302, doi:10.1029/2011JD017048, 2012.

Mlawer, E., Taubman, S., Brown, P., Iacono, M., and Clough, S.: Radiative transfer for inhomogeneous atmospheres: RRTM, a validated correlated-*k* model for the longwave, J. Geophys. Res.-Atmos., 102, 16663–16682, 1997.

Mook, W. G. and van der Plicht, J.: Reporting ^{14}C activities and concentrations, Radiocarbon, 41, 227–239, 1999.

Naegler, T. and Levin, I.: Closing the global radiocarbon budget 1945–2005, J. Geophys. Res., 111, D12311, doi:10.1029/2005JD006758, 2006.

Naegler, T. and Levin, I.: Observation-based global biospheric excess radiocarbon inventory 1963–2005, J. Geophys. Res.-Atmos., 114, D17302, doi:10.1029/2008JD011100, 2009a.

Naegler, T. and Levin, I.: Biosphere-atmosphere gross carbon exchange flux and the $\delta^{13}CO_2$ and $\Delta^{14}CO_2$ disequilibria constrained by the biospheric excess radiocarbon inventory, J. Geophys. Res.-Atmos., 114, D17303, doi:10.1029/2008JD011116, 2009b.

Nakanishi, M. and Niino, H.: An improved Mellor-Yamada level-3 model: its numerical stability and application to a regional prediction of advection fog, Bound.-Lay. Meteorol., 119, 397–407, 2006.

National Centers for Environmental Prediction/National Weather Service/NOAA/U.S. Department of Commerce, 2000: NCEP FNL Operational Model Global Tropospheric Analyses, continuing from July 1999, Research Data Archive at the National Center for Atmospheric Research, Computational and Information Systems Laboratory, Boulder, CO, doi:10.5065/D6M043C6, updated daily, last access: 14 June 2011.

Nydal, R.: Further investigation on the transfer of radiocarbon in nature, J. Geophys. Res., 73, 3617–3635, 1968.

Nydal, R. and Gislefoss, J.: Further application of bomb ^{14}C as a tracer in the atmosphere and ocean, Radiocarbon, 38, 389–406, 1996.

Olivier, J. G. J. and Peters, J. A. H. W.: Uncertainties in global, regional and national emission inventories, in: Non-CO_2 Greenhouse Gases: Scientific Understanding, Control Options and Policy Aspects, edited by: van Ham, J., Baede, A. P. M., Guicherit, R., and Williams-Jacobse, J. F. G. M., Proceedings of the Third International Symposium, Maastricht, Netherlands, 21–23 January 2002, Millpress Science Publishers, Rotterdam, 525–540, ISBN 90-77017-70-4, 2002.

Olsen, S. and Randerson, J.: Differences between surface and column atmospheric CO_2 and implications for carbon cycle research, J. Geophys. Res., 109, D02301, doi:10.1029/2003JD003968, 2004.

Palstra, S. W. L., Karstens, U., Streurman, H., and Meijer, H. A. J.: Wine ethanol ^{14}C as a tracer for fossil fuel CO_2 emissions in Europe: measurements and model comparison, J. Geophys. Res.-Atmos., 113, D21305, doi:10.1029/2008JD010282, 2008.

Peters, W., Krol, M. C., van der Werf, G. R., Houweling, S., Jones, C. D., Hughes, J., Schaefer, K., Masarie, K. A., Jacobson, A. R., Miller, J. B., Cho, C. H., Ramonet, M., Schmidt, M., Ciattaglia, L., Apadula, F., Helta, D., Meinhardt, F., di Sarra, A. G., Piacentino, S., Sferlazzo, D., Aalto, T., Hatakka, J., Strom, J., Haszpra, L., Meijer, H. A. J., Laan, S. V. D., Neubert, R. E. M., Jordan, A., Rodo, X., Morgui, J. A., Vermeulen, A. T., Popa, E., Rozanski, K., Zimnoch, M., Manning, A. C., Leuenberger, M., Uglietti, C., Dolman, A. J., Ciais, P., Heimann, M., and Tans, P. P.: Seven years of recent European net terrestrial carbon dioxide exchange constrained by atmospheric observations, Glob. Change Biol., 16, 1317–1337, doi:10.1111/j.1365-2486.2009.02078.x, 2010.

Peylin, P., Houweling, S., Krol, M. C., Karstens, U., Rödenbeck, C., Geels, C., Vermeulen, A., Badawy, B., Aulagnier, C., Pregger, T., Delage, F., Pieterse, G., Ciais, P., and Heimann, M.: Importance of fossil fuel emission uncertainties over Europe for CO_2 modeling: model intercomparison, Atmos. Chem. Phys., 11, 6607–6622, doi:10.5194/acp-11-6607-2011, 2011.

Pino, D., Vilà-Guerau de Arellano, J., Peters, W., Schröter, J., van Heerwaarden, C. C., and Krol, M. C.: A conceptual framework to quantify the influence of convective boundary layer development on carbon dioxide mixing ratios, Atmos. Chem. Phys., 12, 2969–2985, doi:10.5194/acp-12-2969-2012, 2012.

Pregger, T., Scholz, Y., and Friedrich, R.: Documentation of the Anthropogenic GHG Emission Data for Europe Provided in the Frame of CarboEurope GHG and CarboEurope IP, Final Report CarboEurope-IP, Institute for Energy Economics and the Rational Use of Energy (IER), University of Stuttgart, Germany, 2007.

Randerson, J., Enting, I., Schuur, E., Caldeira, K., and Fung, I. Y.: Seasonal and latitudinal variability of troposphere D $^{14}CO_2$: Post bomb contributions from fossil fuels, oceans, the stratosphere, and the terrestrial biosphere, Global Biogeochem. Cy., 16, 1112, doi:10.1029/2002GB001876, 2002.

Raupach, M., Marland, G., Ciais, P., Quéré, C. L., Canadell, J., Klepper, G., and Field, C.: Global and regional drivers of accelerating CO_2 emissions, P. Natl. Acad. Sci. USA, 104, 10288–10293, doi:10.1073/pnas.0700609104, 2007.

Riley, W., Hsueh, D., Randerson, J., Fischer, M. L., Hatch, J. G., Pataki, D. E., Wang, W., and Goulden, M. L.: Where do fossil fuel carbon dioxide emissions from California go? An analysis based on radiocarbon observations and an atmospheric transport model, J. Geophys. Res., 113, G04002, doi:10.1029/2007JG000625, 2008.

Roberts, M. and Southon, J.: A preliminary determination of the absolute $^{14}C/^{12}C$ ratio of OX-I, Radiocarbon, 49, 441–445, 2007.

Schaefer, K., Collatz, G. J., Tans, P., Denning, A. S., Baker, I., Berry, J., Prihodko, L., Suits, N., and Philpott, A.: Combined simple biosphere/Carnegie–Ames–Stanford approach terrestrial carbon cycle model, J. Geophys. Res.-Biogeo., 113, G03034, doi:10.1029/2007JG000603, 2008.

Shibata, S., Kawano, E., and Nakabayashi, T.: Atmospheric $^{14}CO_2$ variations in Japan during 1982–1999 based on ^{14}C measurements of rice grains, Appl. Radiat. Isotopes, 63, 285–290, doi:10.1016/j.apradiso.2005.03.011, 2005.

Skamarock, W., Klemp, J., Dudhia, J., Gill, D. O., Barker, D. M., Duda, M. G., Huang, X.-Y., Wang, W., and Powers, J. G.: A Description of the Advanced Research WRF Version 3. NCAR Technical Note NCAR/TN-475+STR, doi:10.5065/D68S4MVH, 2008.

Steeneveld, G.-J., Mauritsen, T., Bruijn, E. D., and de Arellano, J. V.-G.: Evaluation of limited-area models for the representation of the diurnal cycle and contrasting nights in CASES-99, J. Appl. Meteorol. Clim., 47, 869–887, 2008.

Stuefer, M., Freitas, S. R., Grell, G., Webley, P., Peckham, S., McKeen, S. A., and Egan, S. D.: Inclusion of ash and SO_2 emissions from volcanic eruptions in WRF-Chem: development and some applications, Geosci. Model Dev., 6, 457–468, doi:10.5194/gmd-6-457-2013, 2013.

Stuiver, M. and Polach, H.: Discussion: reporting of ^{14}C data, Radiocarbon, 19, 355–363, 1977.

Stuiver, M. and Quay, P.: Atmospheric ^{14}C changes resulting from fossil fuel CO_2 release and cosmic ray flux variability, Earth Planet. Sci. Lett., 53, 349–362, 1981.

Suess, H.: Radiocarbon concentration in modern wood, Science, 122, 415–417, 1955.

Svetlik, I., Povinec, P. P., Molnar, M., Vana, M., Sivo, A., and Bujtas, T.: Radiocarbon in the air of central Europe: Long-term investigations, Radiocarbon, 52, 823–834, 2010.

Tie, X., Madronich, S., Li, G., Ying, Z., Weinheimer, A., Apel, E., and Campos, T.: Simulation of Mexico City plumes during the MIRAGE-Mex field campaign using the WRF-Chem model, Atmos. Chem. Phys., 9, 4621–4638, doi:10.5194/acp-9-4621-2009, 2009.

Tolk, L. F., Peters, W., Meesters, A. G. C. A., Groenendijk, M., Vermeulen, A. T., Steeneveld, G. J., and Dolman, A. J.: Modelling regional scale surface fluxes, meteorology and CO_2 mixing ratios for the Cabauw tower in the Netherlands, Biogeosciences, 6, 2265–2280, doi:10.5194/bg-6-2265-2009, 2009.

Turnbull, J., Miller, J., Lehman, S., and Tans, P.: Comparison of $^{14}CO_2$, CO, and SF_6 as tracers for recently added fossil fuel CO_2 in the atmosphere and implications for biological CO_2 exchange, Geophys. Res. Lett., 33, L01817, doi:10.1029/2005GL024213, 2006.

Turnbull, J. C., Miller, J. B., Lehman, S. J., Hurst, D., Peters, W., Tans, P. P., Southon, J., Montzka, S. A., Elkins, J. W., Mondeel, D. J., Romashkin, P. A., Elansky, N., and Skorokhod, A.: Spatial distribution of $\Delta^{14}CO_2$ across Eurasia: measurements from the TROICA-8 expedition, Atmos. Chem. Phys., 9, 175–187, doi:10.5194/acp-9-175-2009, 2009a.

Turnbull, J., Rayner, P., Miller, J., Naegler, T., Ciais, P., and Cozic, A.: On the use of $^{14}CO_2$ as a tracer for fossil fuel CO_2: Quantifying uncertainties using an atmospheric transport model, J. Geophys. Res., 114, D22302, doi:10.1029/2009JD012308, 2009b.

Turnbull, J. C., Karion, A., Fischer, M. L., Faloona, I., Guilderson, T., Lehman, S. J., Miller, B. R., Miller, J. B., Montzka, S., Sherwood, T., Saripalli, S., Sweeney, C., and Tans, P. P.: Assessment of fossil fuel carbon dioxide and other anthropogenic trace gas emissions from airborne measurements over Sacramento, California in spring 2009, Atmos. Chem. Phys., 11, 705–721, doi:10.5194/acp-11-705-2011, 2011.

Turnbull, J., Guenther, D., Karion, A., Sweeney, C., Anderson, E., Andrews, A., Kofler, J., Miles, N., Newberger, T., Richardson, S., and Tans, P.: An integrated flask sample collection system for greenhouse gas measurements, Atmos. Meas. Tech., 5, 2321–2327, doi:10.5194/amt-5-2321-2012, 2012.

van der Laan, S., Karstens, U., Neubert, R., Laan-Luijkx, I. V. D., and Meijer, H.: Observation-based estimates of fossil fuel-derived CO_2 emissions in the Netherlands using ^{14}C, CO and ^{222}Radon, Tellus B, 62, 389–402, doi:10.1111/j.1600-0889.2010.00493.x, 2010.

van der Molen, M. and Dolman, A.: Regional carbon fluxes and the effect of topography on the variability of atmospheric CO_2, J. Geophys. Res., 112, D01104, doi:10.1029/2006JD007649, 2007.

van der Stricht, S. and Janssens, A.: Radioactive effluents from nuclear power stations and nuclear fuel reprocessing sites in the European Union, 2004–2008, Radiat. Prot., 164, ISBN 978-92-79-16922-9, doi:10.2833/27366, 2010.

van der Velde, I. R., Miller, J. B., Schaefer, K., van der Werf, G. R., Krol, M. C., and Peters, W.: Towards multi-tracer data-assimilation: biomass burning and carbon isotope exchange in SiBCASA, Biogeosciences Discuss., 11, 107–149, doi:10.5194/bgd-11-107-2014, 2014.

van Laar, H., Goudriaan, J., and Keulen, H. V.: SUCROS97: simulation of crop growth for potential and water-limited production situations; as applied to spring wheat, Vol. 14, DLO Research Institute for Agrobiology and Soil Fertility and The C. T. de Wit Graduate School for Production Ecology, Wageningen University library, the Netherlands, available at: http://edepot.wur.nl/4426 (last access: 8 July 2014), 1997.

Vermeulen, A. T., Hensen, A., Popa, M. E., van den Bulk, W. C. M., and Jongejan, P. A. C.: Greenhouse gas observations from Cabauw Tall Tower (1992–2010), Atmos. Meas. Tech., 4, 617–644, doi:10.5194/amt-4-617-2011, 2011.

Vilà-Guerau de Arellano, J., Gioli, B., Miglietta, F., Jonker, H. J. J., Baltink, H. K., Hutjes, R. W. A., and Holtslag, A. A. M.: Entrainment process of carbon dioxide in the atmospheric boundary layer, J. Geophys. Res., 109, D18110, doi:10.1029/2004JD004725, 2004.

Vogel, F., Hammer, S., Steinhof, A., Kromer, B., and Levin, I.: Implication of weekly and diurnal ^{14}C calibration on hourly estimates of CO-based fossil fuel CO_2 at a moderately polluted site in southwestern Germany, Tellus B, 62, 512–520, 2010.

Vogel, F., Tiruchittampalam, B., Theloke, J., Kretschmer, R., Gerbig, C., Hammer, S., and Levin, I.: Can we evaluate a fine-grained emission model using high-resolution atmospheric transport modelling and regional fossil fuel CO_2 observations?, Tellus B, 65, 18681, doi:10.3402/tellusb.v65i0.18681, 2013.

Wang, Z., Xiang, Y., and Guo, Q.: ^{14}C levels in tree rings located near Qinshan Nuclear Power Plant, China, Radiocarbon, 54, 2, doi:10.2458/azu_js_rc.v54i2.15869, 2012.

Wang, Z., Xiang, Y., and Guo, Q.: Terrestrial distribution of ^{14}C in the vicinity of Qinshan nuclear power plant, China, Radiocarbon, 55, 59–66, 2013.

Watson, A. J., Schuster, U., Bakker, D. C. E., Bates, N. R., Corbiere, A., Gonzalez-Davila, M., Friedrich, T., Hauck, J., Heinze, C., Johannessen, T., Kortzinger, A., Metzl, N., Olafsson, J., Olsen, A., Oschlies, A., Padin, X. A., Pfeil, B., Santana-Casiano, J. M., Steinhoff, T., Telszewski, M., Rios, A. F., Wallace, D. W. R., and Wanninkhof, R.: Tracking the variable North Atlantic sink for atmospheric CO_2, Science, 326, 1391–1393, doi:10.1126/science.1177394, 2009.

Willmott, C.: Some comments on the evaluation of model performance, B. Am. Meteorol. Soc., 63, 1309–1313, 1982.